

Presented at the International Conference
Strangeness in Quark Matter, held in Padova, July 1998
 To appear in: Journal of Physics G

Chemical Nonequilibrium in High Energy Nuclear Collisions

Jean Letessier

LPTHE, Université Paris 7, 2 pl. Jussieu, F-75251 Cedex 05

Johann Rafelski

Department of Physics, University of Arizona, Tucson, AZ 85721

Abstract. Strange particles produced in S–Au/W/Pb 200 A GeV and Pb–Pb 158 A GeV reactions are described invoking final hadronic phase space in thermal equilibrium, but allowing chemical non-equilibrium. Several sets of statistical freeze-out parameters are obtained for each system, invoking different models of dense matter. We show that only when allowing for strange and non-strange flavor abundance non-equilibrium, a statistically significant description of the experimental results is obtained. Physical properties of the fireball at chemical freeze-out condition are evaluated and considerable universality of hadron freeze-out between the two different collision systems is established. The relevance of the Coulomb effect in the highly charged Pb–Pb fireballs for the chemical analysis are discussed. The influence of explosive collective matter flow is also described.

1. Chemical non-equilibrium statistical model

1.1. Introductory remarks

We report here on the recent progress we made with the thermal model freeze-out analysis of the CERN-SPS 200 A GeV Sulphur beam reactions with laboratory stationary ‘heavy’ targets, such as Gold, Tungsten or Lead nuclei [1], and we also present the current status of our ongoing effort to understand the results from CERN 158 A GeV Lead beam Pb–Pb collisions [2, 3]. These reactions occur at an energy $E_{CM} = \sqrt{s}/B = 8\text{--}9\text{ GeV} \simeq 9m_Nc^2$ per participating nucleon in the center of momentum frame. This high energy available materializes in form of high hadronic particle multiplicity which we are aiming to interpret. In this work we assume local thermal (*i.e.*, energy equipartition) equilibrium [4, 5, 6, 7] reached in a relatively small and dense volume of highly excited hadronic matter, the ‘fireball’. One can argue that the accessibility of many degrees of freedom, as expressed by high specific entropy content, validates thermal equilibrium approach. As of now there is no established theoretical argument for the rapid kinetic equilibration process in highly excited, dense hadronic matter. However, this seems to be the case: consider that as seen in the results of the precise measurements made by experiments WA85/WA94/WA97 [8, 9], the transverse mass spectra are nearly identical for particle-antiparticle pairs where particles comprise some quarks brought into the reaction, *e.g.*, $\bar{\Lambda}-\Lambda$, $\Xi-\bar{\Xi}$. When modeling the production of these particles in microscopic models, we encounter in general vastly different m_\perp spectra [10].

The fireball undergoes complex *chemical* evolution until at some stage final state particle abundances freeze-out. We refer here to the stage in evolution of the fireball at which density has dropped to the level that in subsequent collisions particle abundances remain unchanged. The mechanisms of chemical equilibration in which particle numbers change are today theoretically better understood than are mechanisms responsible for what is believed to be much faster to establish thermal (kinetic) equilibration, where momentum exchange between existent particles is the key mechanism. Recall that it has been the allowance of non-equilibrium chemical abundance for strange quarks which permitted to analyze accurately the experimental strange particle abundance data and to characterize the properties of the particle source [6, 11, 12, 13, 14]. Here our primary result, concluded from the success of the description of the experimental data, is that chemical non-equilibrium both for light and strange quarks is a necessary requisite for the understanding of the experimental particle abundances. The corresponding technical refinement not present in earlier work is that we introduce a parameter, the light quark phase space occupancy (see below) γ_q to describe the light quark chemical non-equilibrium[1, 22]. We did not previously consider simultaneously a interpretation of strange and non-strange particles and hence the need to allow for light quark chemical non-equilibrium was not visible to us: the strange quark phase space occupancy γ_s was determined *relative* to γ_q , which we now understand is also off-equilibrium. Since we now can accurately describe abundances of strange as well as non-strange hadrons, we combine in the present analysis the strangeness diagnostic tools of dense matter with the entropy enhancement [12, 15]. We side-step here initially, mainly to keep the number of parameters to a minimum, the need to study collective matter flows originating in both, the memory of the initial ‘longitudinal’ collision momentum, and the explosive disintegration driven by the internal pressure of compressed hadronic matter. However, we will present in section 5 a short account of the results obtained with such effects, and illustrate changes that arise in our present study.

1.2. Parameters and their physical meaning

We employ the local thermal equilibrium method, and thus use a local freeze-out temperature T_f . Regarding chemical equilibration, we will recognize two different types, relative and absolute. We speak of relative chemical equilibration occurring through quark exchange reactions described in terms of fugacities λ_i , $i = u, d, s$. In general we will not distinguish between the two light $q = u, d$ quarks, and thus we use two fugacities only. From the valance quark fugacities, the hadronic particle fugacities are reconstituted. However, the fugacities λ_i do not regulate the total number of s - \bar{s} valance quark-pairs present, and this number has to be controlled by a new parameter, the phase space occupancies γ_i , $i = u, d, s$ — again, we shall not distinguish between the two light flavors.

To understand the role of γ_i note that any compound particle comprising a particle-antiparticle pair is not controlled in abundance by a fugacity, since the formation of such particles does not impact the conservation laws. The abundance of, *e.g.*, neutral pions comprises normally no (quark) fugacity at all. This abundance is thought to be regulated solely by temperature. This of course implies the tacit assumption of absolute chemical equilibrium. However, the effective fugacity of quarks is $\lambda_i \gamma_i$ and antiquarks $\lambda_i^{-1} \gamma_i$, and thus with the introduction of γ_i we can control pair abundance independently of other properties of the system. The proper

statistical physics foundation of γ_i is obtained considering the maximum entropy principle for evolution of physical systems. In such a study it has been determined that while the equilibrium limit $\gamma_i \rightarrow 1$ maximizes the specific chemical entropy, this maximum is very shallow [16], indicating that a system with dynamically evolving physical properties such as the occupied volume will in general find more effective paths to increase entropy, than offered by the establishment of the absolute chemical equilibrium.

The dynamical theory for γ_s has been one of the early cornerstones of the proposal to use strangeness as signature of deconfinement [17, 18]. A time dependent build up of chemical abundance was first considered in the context of microscopic strangeness production in QGP, after it was realized that strange flavor production occurs at the same time scale as the collision process. More generally, one must expect, considering the time scales, that all quark flavors will not be able to exactly follow the rapid evolution in time of dense hadronic matter. Moreover, fragmentation of gluons in hadronizing QGP can contribute additional quark pair abundance, conveniently described by the factor γ_i . It is thus to be expected that also for light quarks the chemical phase space occupancy factor $\gamma_q \neq 1$. Introduction of the factor γ_q leads to a precise chemical description of the S–Au/W/Pb 200 A GeV collisions [1], which was not possible before. The tacit choice $\gamma_q = 1$ has not allowed previously to distinguish the different reaction scenarios in Pb–Pb collisions leading to contradictory results [2, 14]. Introduction of γ_q , along with improvement in experimental precision, and a greater data sample, allows to develop the here presented precise analysis.

1.3. Hadronic phase space

The evaluation of the final particle yields follows the pattern established in our earlier work (see, *e.g.*, [6]). The relative number of primary particles freezing out from a source is obtained noting that the fugacity and phase space occupancy of a composite hadronic particle is expressed by its constituents and that the probability to find all j -components contained within the i -th emitted particle is:

$$N_i \propto \prod_{j \in i} \gamma_j \lambda_j e^{-E_j/T}, \quad \lambda_i = \prod_{j \in i} \lambda_j, \quad \gamma_i = \prod_{j \in i} \gamma_j. \quad (1)$$

The unstable hadronic resonances are allowed to disintegrate and feed the stable hadron spectra. Full phase space coverage or central rapidity region $|y - y_{\text{CM}}| < 0.5$, is considered, where as usual the energy of the particles is expressed by

$$E_j = \sqrt{m_j^2 + p^2} = \sqrt{m_j^2 + p_\perp^2} \cosh y,$$

and y_{CM} is the center of momentum rapidity of the colliding nuclei.

Hadron spectra are not significantly deformed by cascading decays of heavier resonances at sufficiently high p_\perp , and all small acceptance particle ratios we consider are thus chosen to satisfy well this criterion. Therefore, in our approach, we first evaluate the partial multiplicities for different hadrons within the acceptance domain, and allow these to decay to obtain the contributing fraction. In principle the approach must be to take the momentum distribution of primary particles, have the momentum distribution cascade into secondaries which may again cascade. Only the final abundance is then kinematically cut to the experimental acceptance. Unless a random simulation is carried out (unsuitable for rarely produced particles we are interested in), this approach is completely impossible numerically: at each level of

cascading there is a new level of averaging over the phase space in addition to the one needed when treating the flow, see below, and thus normally only ONE decay step is accounted for. Our approach thus has the advantage of incorporating multi-step cascading effects, at the cost of somewhat inaccurate implementation of cuts. However, we believe, and have checked in so far possible, that the theoretical uncertainties our approach introduces are much smaller than the experimental errors.

Once the parameters T_f , λ_q , λ_s , γ_q , γ_s are determined from the particle yields available, we can reconstitute the entire hadronic particle phase space and obtain the physical properties of the system, such as, *e.g.*, energy and entropy per baryon, strangeness content. Even though we are describing a free streaming gas of emitted particles, we can proceed as if we were evaluating partition function of system with the phase space distribution described by the statistical parameters, given that just in an earlier instant in a gedanken experiment we have a cohesive, interacting system. We have implemented all relevant hadronic states and resonances in this approach and have also included quantum statistical corrections, allowing for first Bose and Fermi distribution corrections in the hadron abundances and in the phase space content. These corrections influence favorably the quality of the agreement between theory and experiment.

1.4. Inclusion of collective flow

Most of our analysis will be carried out under the assumption that the effects of matter flow can be accommodated later, since the 4π particle ratios are not influenced, and the ratios of compatible particles (*i.e.*, those dragged along by matter in the same manner, *viz*, strange baryons and antibaryons) are not affected significantly. While this is correct in general, the precision of the experimental data at this time requires a more detailed study, for the flow also depends on particle mass and strange (anti)baryons differ by nearly 50% comparing Λ with Ω . Thus, in section 5, we shall briefly discuss the effect a collective matter flow flow velocity \vec{v}_c at chemical freeze-out has on our analysis. Several different schemes to implement flow were studied previously [19]. As our example we adopt here a radial expansion model and consider the causally disconnected domains of the dense matter fireball to be synchronized at the instance of collision — in other words the time of freeze-out is for all volume elements a common constant time in the CM frame. The freeze-out occurs at the surface of the fireball simultaneously in the CM frame, but not necessarily within a short instant of CM-time. Since we do not use a radial profile of the flow velocity in the fireball, it amounts to the tacit assumption that all hadrons are born at same surface velocity as would be the case were the chemical freeze-out condition also the QGP-hadronization condition.

Within this approach the spectra and thus also multiplicities of particles emitted are obtained replacing the Boltzmann factor in Eq. (1) by:

$$e^{-E_j/T} \rightarrow \frac{1}{2\pi} \int d\Omega_v \gamma_v (1 + \vec{v}_c \cdot \vec{p}_j/E_j) e^{-\frac{\gamma_v E_j}{T} (1 + \vec{v}_c \cdot \vec{p}_j/E_j)}, \quad (2)$$

where as usual $\gamma_v = 1/\sqrt{1 - \vec{v}_c^2}$. Eq. (2) can be intuitively obtained by a Lorentz transformation between an observer on the surface of the fireball, and one at rest in laboratory frame. In certain details the results we obtain confirm the applicability of this simple approach.

As can be seen in Eq. (2) we need to carry out an additional two dimensional (half-sphere) surface integral with the coordinate system fixed by an arbitrary, but

Table 1. Particle ratios studied in our analysis for S–W/Pb/Au reactions: experimental results with references and kinematic cuts are given, followed by columns showing results for the different strategies of analysis B–F. Asterisk $*$ means a predicted result (corresponding data is not fitted). The experimental results here considered are from

- ¹ S. Abatzis *et al.*, WA85 Collaboration, *Heavy Ion Physics* **4**, 79 (1996).
- ² S. Abatzis *et al.*, WA85 Collaboration, *Phys. Lett. B* **347**, 158 (1995).
- ³ S. Abatzis *et al.*, WA85 Collaboration, *Phys. Lett. B* **376**, 251 (1996).
- ⁴ I.G. Bearden *et al.*, NA44 Collaboration, *Phys. Rev. C* **57**, 837 (1998).
- ⁵ D. Röhrl for the NA35 Collaboration, *Heavy Ion Physics* **4**, 71 (1996).
- ⁶ S–Ag value adopted here: T. Alber *et al.*, NA35 Collaboration, *Eur. Phys. J. C* **2**, 643 (1998); [hep-ex/9711001].
- ⁷ A. Iyono *et al.*, EMU05 Collaboration, *Nucl. Phys. A* **544**, 455c (1992) and Y. Takahashi *et al.*, EMU05 Collaboration, private communication.

Ratios	Ref.	Cuts[GeV]	Exp.Data	B	C	D	D _s	F
Ξ/Λ	1	$1.2 < p_\perp < 3$	0.097 ± 0.006	0.16	0.11	0.099	0.11	0.10
$\Xi/\bar{\Lambda}$	1	$1.2 < p_\perp < 3$	0.23 ± 0.02	0.38	0.23	0.22	0.18	0.22
$\bar{\Lambda}/\Lambda$	1	$1.2 < p_\perp < 3$	0.196 ± 0.011	0.20	0.20	0.203	0.20	0.20
Ξ/Ξ	1	$1.2 < p_\perp < 3$	0.47 ± 0.06	0.48	0.44	0.45	0.33	0.44
$\bar{\Omega}/\Omega$	2	$p_\perp > 1.6$	0.57 ± 0.41	1.18*	0.96*	1.01*	0.55*	0.98
$\frac{\Omega+\bar{\Omega}}{\Xi+\bar{\Xi}}$	2	$p_\perp > 1.6$	0.80 ± 0.40	0.27*	0.17*	0.16*	0.16*	0.16
K^+/K^-	1	$p_\perp > 0.9$	1.67 ± 0.15	2.06	1.78	1.82	1.43	1.80
K_s^0/Λ	3	$p_\perp > 1$	1.43 ± 0.10	1.56	1.64	1.41	1.25	1.41
$K_s^0/\bar{\Lambda}$	3	$p_\perp > 1$	6.45 ± 0.61	7.79	8.02	6.96	6.18	6.96
K_s^0/Λ	1	$m_\perp > 1.9$	0.22 ± 0.02	0.26	0.28	0.24	0.24	0.24
$K_s^0/\bar{\Lambda}$	1	$m_\perp > 1.9$	0.87 ± 0.09	1.30	1.38	1.15	1.20	1.16
Ξ/Λ	1	$m_\perp > 1.9$	0.17 ± 0.01	0.27	0.18	0.17	0.18	0.17
$\Xi/\bar{\Lambda}$	1	$m_\perp > 1.9$	0.38 ± 0.04	0.64	0.38	0.38	0.30	0.37
$\frac{\Omega+\bar{\Omega}}{\Xi+\bar{\Xi}}$	1	$m_\perp > 2.3$	1.7 ± 0.9	0.98*	0.59*	0.58*	0.52*	0.58
p/\bar{p}	4	Mid-rapidity	11 ± 2	11.2	10.1	10.6	7.96	10.5
$\bar{\Lambda}/\bar{p}$	5	4π	1.2 ± 0.3	2.50	1.47	1.44	1.15	1.43
$\frac{h^-}{p-\bar{p}}$	6	4π	4.3 ± 0.3	4.4	4.2	4.1	3.6	4.1
$\frac{h^+ - h^-}{h^+ + h^-}$	7	4π	0.124 ± 0.014	0.11	0.10	0.103	0.09	0.10
		χ_T^2		264	30	6.5	38	12

fixed (collision) axis which defines the transverse particle momentum. Just a one dimensional numerical integration over one of the surface angles needs to be carried out. To obtain the particle spectra as function of m_\perp we need also to integrate over rapidity y . This rapidity integration can be approximated for a narrow rapidity interval using the error function.

2. Experimental results and the data analysis

We consider for S–Au/W/Pb reactions 18 data points listed in table 1 (of which three comprise the Ω 's). For Pb–Pb we address here 15 presently available particle yield ratios listed in table 2 (of which four comprise the Ω 's). We believe to have included in our discussion most if not all particle multiplicity results available presently.

The particle data shown in tables 1 and 2 are obtained looking for a set of physical parameters which will minimize the difference between theory and experiment. This

Table 2. Particle ratios studied in our analysis for Pb–Pb reactions: experimental results with references and kinematic cuts are given, followed by columns showing results for the different strategies of analysis B–F. Asterisk * means a predicted result (corresponding data is not fitted or not available). The experimental results here considered are from

- ¹ I. Králik, for the WA97 Collaboration, *Nucl. Phys. A* (1998) (presented at Tsukuba QM1998 meeting).
- ² G.J. Odyniec, for the NA49 Collaboration, *J. Phys. G* **23**, 1827 (1997).
- ³ P.G. Jones, for the NA49 Collaboration, *Nucl. Phys. A* **610**, 188c (1996).
- ⁴ F. Pühlhofer, for the NA49 Collaboration, *Nucl. Phys. A* (1998) (presented at Tsukuba QM1998 meeting).
- ⁵ C. Bormann, for the NA49 Collaboration, *J. Phys. G* **23**, 1817 (1997).
- ⁶ G.J. Odyniec, *Nucl. Phys. A* (1998) (presented at Tsukuba QM1998 meeting).
- ⁷ D. Röhrlig, for the NA49 Collaboration, “Recent results from NA49 experiment on Pb–Pb collisions at 158 A GeV”, see Fig. 4, in proc. of EPS-HEP Conference, Jerusalem, Aug. 19–26, 1997.
- ⁸ A.K. Holme, for the WA97 Collaboration, *J. Phys. G* **23**, 1851 (1997).

Ratios	Ref.	Cuts[GeV]	Exp.Data	B	C	D	D _s	F
Ξ/Λ	1	$p_{\perp} > 0.7$	0.099 ± 0.008	0.138	0.093	0.095	0.098	0.107
$\bar{\Xi}/\bar{\Lambda}$	1	$p_{\perp} > 0.7$	0.203 ± 0.024	0.322	0.198	0.206	0.215	0.216
$\bar{\Lambda}/\Lambda$	1	$p_{\perp} > 0.7$	0.124 ± 0.013	0.100	0.121	0.120	0.119	0.121
$\bar{\Xi}/\Xi$	1	$p_{\perp} > 0.7$	0.255 ± 0.025	0.232	0.258	0.260	0.263	0.246
$\frac{(\Xi+\bar{\Xi})}{(\Lambda+\bar{\Lambda})}$	2	$p_{\perp} > 1.$	0.13 ± 0.03	0.169	0.114	0.118	0.122	0.120
K_s^0/ϕ	3,4		11.9 ± 1.5	6.3	10.4	9.89	9.69	16.1
K^+/K^-	5		1.80 ± 0.10	1.96	1.75	1.76	1.73	1.62
p/\bar{p}	6		$18.1 \pm 4.$	22.0	17.1	17.3	17.9	16.7
$\bar{\Lambda}/\bar{p}$	7		$3. \pm 1.$	3.02	2.91	2.68	3.45	0.65
K_s^0/B	3		0.183 ± 0.027	0.305	0.224	0.194	0.167	0.242
h^-/B	3		1.83 ± 0.2	1.47	1.59	1.80	1.86	1.27
Ω/Ξ	1	$p_{\perp} > 0.7$	0.192 ± 0.024	0.119*	0.080*	0.078*	0.080*	0.192
$\bar{\Omega}/\bar{\Xi}$	8	$p_{\perp} > 0.7$	0.27 ± 0.06	0.28*	0.17*	0.17*	0.18*	0.40
$\bar{\Omega}/\Omega$	1	$p_{\perp} > 0.7$	0.38 ± 0.10	0.55*	0.56*	0.57*	0.59*	0.51
$\frac{(\Omega+\bar{\Omega})}{(\Xi+\bar{\Xi})}$	8	$p_{\perp} > 0.7$	0.20 ± 0.03	0.15*	0.10*	0.10*	0.10*	0.23
		χ^2_{Γ}		88	24	1.6	2.7	19

minimization is accomplished using the MINUIT96.03 program package from the CERN Fortran library. Several approaches to data analysis were tested in order to show the relevance of the different physical effects we discussed above. In the approach B we keep to the chemical equilibrium and thus allow for a search amongst three parameters, T_f , λ_q , and λ_s leaving the two non-equilibrium chemical parameters at their equilibrium value ($\gamma = 1$). This is the so-called hadronic gas model, and it fails. In the approach C we introduce strangeness chemical non-equilibrium, *i.e.*, we also vary γ_s and in D we also vary the light quark non-equilibrium abundance parameter γ_q searching for best agreement between theory and experiment. In fit F we include the particle abundances comprising the triply strange $\Omega, \bar{\Omega}$ particles. These particles are found in the S–Au/W/Au system to give a slight difficulty, despite their great measurement errors. In the Pb–Pb case we see in table 2 that there is a systematic deviation not accounted even in the here presented non-equilibrium model. The particle ratios comprising Ω and $\bar{\Omega}$ -particles do not follow the same systematics. This can be also seen in particle spectra inverse slopes presented by

Table 3. Statistical parameters which best describe the experimental S–Au/W/Pb results shown in table 1. Asterisk (*) means a fixed (input) value or result of a constraint. In approaches B to D, particle abundance ratios comprising Ω are not considered. In case D_s strangeness conservation in the particle yields was enforced. In case F the three data-points with Ω are considered.

Fits	T_f [MeV]	λ_q	λ_s	γ_s/γ_q	γ_q	χ_T^2
B	144 ± 2	1.53 ± 0.02	0.97 ± 0.02	1^*	1^*	264
C	147 ± 2	1.49 ± 0.02	1.01 ± 0.02	0.62 ± 0.02	1^*	30
D	143 ± 3	1.50 ± 0.02	1.00 ± 0.02	0.60 ± 0.02	1.22 ± 0.06	6.5
D_s	153 ± 3	1.42 ± 0.02	$1.10^* \pm 0.02$	0.56 ± 0.02	1.26 ± 0.06	38
F	144 ± 3	1.49 ± 0.02	1.00 ± 0.02	0.60 ± 0.02	1.22 ± 0.06	12

the WA97 collaboration [9]. A possible hypothesis is that a good fraction of these particles are made in processes that are different in nature than those leading to the other particle abundances.

In general we have not enforced the strangeness conservation among the emitted hadrons in the phase space. Setting $\langle s - \bar{s} \rangle = 0$ introduces a constraint between parameters which is difficult to satisfy for S-induced reactions, where the particle abundances are obtained at relatively high p_\perp , and thus only a small fraction of all strange particles is actually observed. This constraint is relatively easily satisfied for the Pb–Pb collision results, where a much greater proportion of all strange particles is actually experimentally detected. Fits comprising the strangeness conservation are marked by sub-script ‘s’, and for space reasons we only present here results for the full non-equilibrium case D_s .

We show also at the bottom of tables 1 and 2 the overall relative error:

$$\chi_T^2 = \sum_j \left(\frac{R_{\text{th}}^j - R_{\text{exp}}^j}{\Delta R_{\text{exp}}^j} \right)^2, \quad (3)$$

for all the particles considered (18 or 15 without Omegas for S–Au/W/Pb, and respectively 15 or 11 without Omegas for Pb–Pb). Some of the considered data points can be obtained from others in terms of their definitions, there are two types of relations:

$$\frac{\Omega + \bar{\Omega}}{\Xi + \bar{\Xi}} = \frac{\bar{\Omega}}{\Xi} \cdot \frac{1 + \bar{\Omega}/\Omega}{1 + \bar{\Xi}/\Xi}, \quad \frac{\bar{\Lambda}}{\Lambda} = \frac{\bar{\Lambda}}{\Xi} \cdot \frac{\Xi}{\bar{\Xi}} \cdot \frac{\Xi}{\Lambda}, \quad (4)$$

and for this reason is not trivial to determine the confidence level that goes with the different schemes B–F. However, due to smallness of the total error found for the chemical nonequilibrium cases, it is clear that only these have relatively high statistical significance, and we do not need to go into deeper arguments to see which of the options presented have negligible confidence level, and which deserve to be considered as physically interesting: for S–Au/W/Pb significant is case D (chemical nonequilibrium, no strangeness conservation and no Ω in fit) and to lesser degree fit F (same, but with with Ω). Notable is that the case D_s (strangeness conservation enforced) fails. In Pb–Pb reactions again the case D is acceptable, as is the also D_s in which we force strangeness conservation, but case F which includes the Ω data points fails.

The statistical parameters yielding best particle multiplicities for the S-induced reactions are shown in the table 3. In table 4 we show the corresponding Pb–Pb

Table 4. Statistical parameters which best describe the experimental Pb–Pb results shown in table 2. For definition and role of $\lambda_Q^{-1/3}$ see section 3. Asterisk (*) means a fixed (input) value, or result of a constraint. In approaches B to D, particle abundance ratios comprising Ω are not considered. In case D_s strangeness conservation in the particle yields was enforced. In case F the four data-points with Ω are considered.

Fit	$T_f [MeV]$	$\lambda_q \lambda_Q^{1/6}$	$\lambda_s \lambda_Q^{1/3}$	γ_s/γ_q	γ_q	χ_T^2
B	142 ± 3	1.70 ± 0.03	1.10 ± 0.02	1^*	1^*	88
C	144 ± 4	1.62 ± 0.03	1.10 ± 0.02	0.63 ± 0.04	1^*	24
D	134 ± 3	1.62 ± 0.03	1.10 ± 0.02	0.69 ± 0.08	1.84 ± 0.30	1.6
D _s	133 ± 3	1.63 ± 0.03	$1.09^* \pm 0.02$	0.72 ± 0.12	2.75 ± 0.35	2.7
F	334 ± 18	1.61 ± 0.03	1.12 ± 0.02	0.50 ± 0.01	0.18 ± 0.02	19

parameters. We note that the individual phase space occupancies in Pb–Pb case change drastically between cases D and D_s, however the ratio of the nonequilibrium parameters γ_s/γ_q barely changes from 0.69 to 0.72. In actual numerical procedure we took advantage of this stability in γ_s/γ_q -ratio. In the case of S-induced reactions this ratio is seen to come out slightly smaller and like the quark fugacities, it is relatively stable for all different strategies to interpret the experimental results.

Notable among the values of statistical parameters is the remarkable result $\lambda_s \simeq 1$ in the S–Au/W/Pb case, see table 3. This result requires considerable attention. We recall that the fugacities λ_j arise from conservation laws, in our context, of quark (baryon) number and strangeness in the particle source. $\lambda_q \equiv e^{\mu_q/T}$ is thus the fugacity of the valance light quarks. For a nucleon $\lambda_N = \lambda_q^3$, and hence the baryochemical potential is: $\mu_b = 3\mu_q$. In another refinement both *u*, *d*-flavor fugacities λ_u and λ_d can be introduced, allowing for up-down-quark asymmetry. We recall that by definition $2\mu_q = \mu_d + \mu_u$, thus $\lambda_q \equiv \sqrt{\lambda_u \lambda_d}$. We have implemented one correction related to this refinement, since in the experimental data only the $\Xi^-(ssd)$ particle is measured.

Returning again to strangeness fugacity: for strange quarks we have $\lambda_s \equiv e^{\mu_s/T}$. For an antiparticle fugacity $\lambda_{\bar{s}} = \lambda_s^{-1}$. Some papers refer in this context to hypercharge fugacity $\lambda_S = \lambda_q/\lambda_s$, thus $\mu_S = \mu_q - \mu_s$. This is a highly inconvenient historical definition arising from considerations of a hypothetical hadron gas phase. It hides from view important symmetries, such as $\lambda_s \rightarrow 1$ for a state in which the phase space size for strange and anti-strange quarks is the same: at finite baryon density the number of hyperons is always greater than the number of anti-hyperons and thus the requirement $\langle N_s - N_{\bar{s}} \rangle = 0$ can only be satisfied for some nontrivial $\lambda_s(\lambda_q) \neq 1$. Thus even a small deviation from $\lambda_s \rightarrow 1$ limit must be fully understood in order to argue that the source is deconfined. Conversely, observation of $\lambda_s \simeq 1$ consistently at different experimental conditions is a strong and convincing argument that at least the strange quarks are unbound, *i.e.*, deconfined.

3. Coulomb effect

So how do we explain the fact that Pb–Pb shows definitive deviation from the canonical value $\lambda_s \rightarrow 1$ associated with QGP? The answer has been keeping us for quite a while busy and only recently the obvious resolution has been found: for the highly

Coulomb-charged fireballs formed in Pb–Pb collisions a further effect which needs consideration is the distortion of the particle phase space by the Coulomb potential. This effect influences particles and antiparticles in opposite way, and has by factor two different strength for u -quark (charge $+2/3|e|$) and (d, s) -quarks (charge $-1/3|e|$). Because Coulomb-effect acts in opposite way on u and d quarks, its net impact on λ_q is relatively small as we shall see.

On the other hand, the Coulomb effect distorts significantly the expectation regarding $\lambda_s \rightarrow 1$ for strangeness-deconfined source with vanishing net strangeness. The difference between strange and anti-strange quark numbers (net strangeness) allowing for a Coulomb potential within a relativistic Thomas-Fermi phase space occupancy model [20], allowing for finite temperature in QGP is:

$$\begin{aligned} \langle N_s - N_{\bar{s}} \rangle = \int_{R_f} g_s \frac{d^3 r d^3 p}{(2\pi)^3} & \left[\frac{1}{1 + \gamma_s^{-1} \lambda_s^{-1} e^{(E(p) - \frac{1}{3}V(r))/T}} \right. \\ & \left. - \frac{1}{1 + \gamma_s^{-1} \lambda_s e^{(E(p) + \frac{1}{3}V(r))/T}} \right], \end{aligned} \quad (5)$$

which clearly cannot vanish for $V \neq 0$ in the limit $\lambda_s \rightarrow 1$. In Eq. (5) the subscript R_f on the spatial integral reminds us that only the classically allowed region within the fireball is covered in the integration over the level density; $E = \sqrt{m^2 + \vec{p}^2}$, and for a uniform charge distribution within a radius R_f of charge Z_f :

$$V = \begin{cases} -\frac{3}{2} \frac{Z_f e^2}{R_f} \left[1 - \frac{1}{3} \left(\frac{r}{R_f} \right)^2 \right], & \text{for } r < R_f; \\ -\frac{Z_f e^2}{r}, & \text{for } r > R_f. \end{cases} \quad (6)$$

One obtains a rather precise result for the range of parameters of interest to us (see below) using the Boltzmann approximation:

$$\langle N_s - N_{\bar{s}} \rangle = \gamma_s \left\{ \int g_s \frac{d^3 p}{(2\pi)^3} e^{-E/T} \right\} \int_{R_f} d^3 r \left[\lambda_s e^{\frac{V}{3T}} - \lambda_s^{-1} e^{-\frac{V}{3T}} \right]. \quad (7)$$

The Boltzmann limit allows also to verify the signs: the Coulomb potential is negative for the negatively charged s -quarks with the magnitude of the charge, $1/3$, made explicit in the potential terms in all expressions above. It turns out that there is always only one solution, with resulting $\lambda_s > 1$. The magnitude of the effect is quite significant: choosing $R_f = 8$ fm, $T = 140$ MeV, $m_s = 200$ MeV (value of $0.5 < \gamma_s < 2$ is irrelevant) solution of Eq. (5) for $Z_f = 150$ yields $\lambda_s = 1.10$ (precisely: 1.0983, 1.10 corresponds to $R_f = 7.87$ fm). The remarkable result we found from experimental data is indeed this value $\lambda_s = 1.10 \pm 0.02$, see table 4. Thus also in Pb–Pb system as before for the lighter system S–Au/W/Pb [11, 12] we are finding that the source of strange hadrons is governed by a symmetric (up to Coulomb-asymmetry), and thus presumably deconfined strange quark phase space.

To better understand the situation it is convenient to introduce a charge conservation fugacity λ_Q . The abundance of charged quarks is thus counted by the fugacities:

$$\begin{aligned} \lambda_s & \equiv \tilde{\lambda}_s \lambda_Q^{-1/3}, & \lambda_d & \equiv \tilde{\lambda}_d \lambda_Q^{-1/3}, & \lambda_u & \equiv \tilde{\lambda}_u \lambda_Q^{2/3}, \\ \lambda_q & \equiv \tilde{\lambda}_q \lambda_Q^{1/6} = \sqrt{\lambda_u \lambda_d}. \end{aligned} \quad (8)$$

Given that quark flavor is conserved, and thus charge is conserved implicitly too, λ_Q is not another independent statistical variable, it is determined by the Coulomb potential:

$$\lambda_Q \equiv \frac{\int_{R_f} d^3r e^{\frac{V}{T}}}{\int_{R_f} d^3r} . \quad (9)$$

The difference between λ_q and $\tilde{\lambda}_q$, see Eq. (8), is at the level of 1–2% considering the Pb–Pb case, and yet smaller for S–A reactions. However, the individual light quark fugacities experience more significant shifts as we saw for λ_s . This means that the predictions we and others have made, ignoring the Coulomb effect, for strange particle ratios need improvement. Specifically, the Pb–Pb Coulomb correction factor for the QGP-ratios is (previously predicted ratios i are to be multiplied by f_i): $f_{\Xi/\Lambda} = 1/f_{\Xi/\Lambda} = f_{\bar{\Omega}/\Xi} = 1/f_{\Omega/\Xi} = \lambda_Q^{1/3} \simeq 0.91 \pm 0.02$, $f_{\bar{\Lambda}/\Lambda} = \lambda_Q^{2/3} \simeq 0.83 \pm 0.03$, $f_{\Xi/\Xi} = \lambda_Q^{4/3} \simeq 0.68 \pm 0.05$, $f_{\bar{\Omega}/\Omega} = \lambda_Q^{6/3} \simeq 0.56 \pm 0.07$. This correction is required, since previous studies of QGP state properties referred to the tilde-fugacities, while data analysis where obtained for the non-tilde fugacities, see, *e.g.*, Ref.[2]. Even though charge conservation has been enforced previously [14], this was done without allowance for the Coulomb deformation of the phase space and hence there was no net difference between tilde and non-tilde quantities for large systems. We conclude that a QGP source in order to conserve strangeness has indeed $\tilde{\lambda}_s = 1$, which implies $\lambda_s = \lambda_Q^{-1/3}$, and moreover [11]:

$$\frac{\langle d - \bar{d} \rangle}{\langle u - \bar{u} \rangle} = \frac{2A - Z}{A + Z} = \frac{\tilde{\mu}_d}{\tilde{\mu}_u} = \frac{\ln \tilde{\lambda}_d}{\ln \tilde{\lambda}_u} . \quad (10)$$

For Pb–Pb collisions with $A = 208$ and $Z = 82$ there is indeed a non-negligible isospin asymmetry, but the Coulomb effect slightly over-compensates it and hence $\mu_u > \mu_d$, while $\tilde{\mu}_u < \tilde{\mu}_d$.

4. Physical properties of the fireball at chemical freeze-out

Given the precise statistical information about the properties of the hadron phase space provided in particular by the non-equilibrium case D, we can determine the specific content in energy, entropy, strangeness contained in all hadronic particles, see tables 5 and 6. We show here for the study cases B–F, along with their temperature the specific energy and entropy content, and specific anti-strangeness content, along with specific strangeness asymmetry, and finally pressure at freeze-out, evaluated by using the best statistical parameters to characterize the hadronic particle phase space. We note that it is improper in general to refer to these properties as those of a ‘hadronic gas’ formed in nuclear collisions, as the particles considered may be emitted in sequence from a deconfined source, and thus there never is a stage corresponding to a hadron gas phase.

Strangeness balance is well established only in the Pb–Pb data, and thus it is likely that the difficulty to balance strangeness in the S–Au/W/Pb is really a reflection on the high P_\perp cuts inherent in these experimental results, which had to be obtained against the background of many soft spectator particles, given the non-symmetric collision system considered. The specific \bar{s} content is determined to be 0.90 ± 0.04 in S–Au/W/Pb case and it is noticeably less, 0.61 ± 0.04 for the Pb–Pb collisions. This may be perhaps attributable to greater baryon content of the Pb–formed fireballs, and/or,

Table 5. T_f and physical properties (specific energy, entropy, anti-strangeness, net strangeness, pressure and volume) of the full hadron phase space characterized by the statistical parameters given in table 3 for the reactions S–Au/W/Pb. Asterisk * means fixed input.

Fits	T_f [MeV]	E_f/B	S_f/B	\bar{s}_f/B	$(\bar{s}_f - s_f)/B$	P_f [GeV/fm 3]
B	144 ± 2	8.9 ± 0.5	50 ± 3	1.66 ± 0.06	0.44 ± 0.02	0.056 ± 0.005
C	147 ± 2	9.3 ± 0.5	49 ± 3	1.05 ± 0.05	0.23 ± 0.02	0.059 ± 0.005
D	143 ± 3	9.1 ± 0.5	48 ± 3	0.91 ± 0.04	0.20 ± 0.02	0.082 ± 0.006
D_s	153 ± 3	8.9 ± 0.5	45 ± 3	0.76 ± 0.04	0^*	0.133 ± 0.008
F	144 ± 2	9.1 ± 0.5	48 ± 3	0.91 ± 0.05	0.20 ± 0.02	0.082 ± 0.006

Table 6. T_f and physical properties (specific energy, entropy, anti-strangeness, net strangeness, pressure and volume) of the full hadron phase space characterized by the statistical parameters given in table 4 for the reactions Pb–Pb. Asterisk * means fixed input.

Fit	T_f [MeV]	E_f/B	S_f/B	\bar{s}_f/B	$(\bar{s}_f - s_f)/B$	P_f [GeV/fm 3]
B	142 ± 3	7.1 ± 0.5	41 ± 3	1.02 ± 0.05	0.21 ± 0.02	0.053 ± 0.005
C	144 ± 4	7.7 ± 0.5	42 ± 3	0.70 ± 0.05	0.14 ± 0.02	0.053 ± 0.005
D	134 ± 3	8.3 ± 0.5	47 ± 3	0.61 ± 0.04	0.08 ± 0.01	0.185 ± 0.012
D_s	133 ± 3	8.7 ± 0.5	48 ± 3	0.51 ± 0.04	0^*	0.687 ± 0.030
F	334 ± 18	9.8 ± 0.5	24 ± 2	0.78 ± 0.05	0.06 ± 0.01	1.64 ± 0.006

somewhat lower available energy, in case D we find a difference of 0.8 GeV per nucleon in the CM frame. The second explanation may be more to the point considering that in the S–S case for which we have yet slightly higher energy available in the collision, yet higher strangeness content can be qualitatively inferred [21]. Thus we question if it could be that the energy of CERN experiments is just barely at the critical value and that every small energy increase matters? This invites an experimental test, since very probably with sufficient effort more energetic Pb–SPS beams could be achieved.

The specific entropy content also drops slightly for Pb–Pb (45 ± 3) compared with S–Au/W/Pb (48 ± 3) for the best case D — these values agree well with the entropy content evaluation made earlier [15]. This is so because the abundances of (predominantly high p_\perp) strange particle data are indeed found in this study to be fully consistent within a chemical-nonequilibrium description with the 4π total particle multiplicity results. The pressure of the hadronic phase space in high confidence cases $P_f \simeq 0.1\text{--}0.2 \text{ GeV/fm}^3$ has the magnitude of the vacuum confinement pressure (bag constant).

We do not present here the highly strategy sensitive freeze-out volume V_f , which can be determined assuming that the hadronic phase space comprises for the S–Au/W/Pb collisions baryon number $B \simeq 120$, and in Pb–Pb case being $B \simeq 372 \pm 10$, as stated in [14]. However, we find that a spherical source corresponding to the best case D in case of Pb–Pb reactions would have a source radius 9.6 fm, which in turn can be checked to be in agreement with deconfined strangeness conservation as described by Eq.(5), given the established statistical parameters and $m_s = 200$ MeV.

Comparing the two tables 5 and 6 we note similarities in results which become more clear when we study the extensive physical properties of the two freeze-out

systems. We choose a fixed given value of the freeze-out temperature $T_f \in (125\text{--}200)$ MeV and find best values of the other parameters according to the strategy D, and evaluate for both systems extensive physical properties. This comparison yields a surprise shown in figure 1. We see that solid lines (case of Pb–Pb) are crossing dashed lines (case of S–Au/W/Pb) at nearly the same value of $T_f \simeq 143$ MeV. Thus it appears possible that a universal freeze-out for these and other similar collision systems arises, corresponding possibly to the common physical properties of QGP at its breakup into hadrons — in this context we draw attention to the interesting result about the scale of the energy density at freeze-out: $\epsilon_f = 0.43 \pm 0.04 \text{ GeV/fm}^3$. These results, along with earlier shown strange phase space symmetry and the Coulomb effect in the Pb–Pb system has as simple interpretation the formation of a deconfined phase in the initial stages of the collision, which subsequently evolves and flows apart till it reaches the universal hadronization point, with many similar physical properties, independent of the collision system. System dependent will certainly the surface collective velocity \vec{v}_c .

5. Collective flow

So far we have considered only the particle yields, and have not addressed particle spectra which requires that we allow for the Doppler-like blue shift of the particles emitted from a moving source at hadronization. To do this quantitatively we need to consider explicitly the collective velocity \vec{v}_c , see section 1.4. Moreover, while the integral over the entire phase space of the flow spectrum yields as many particles with and without flow, when acceptance cuts are present particles of different mass experience differing flow effects. While we made an effort to avoid forming ratios of particles which are subject to greatly differing flow effects, we must expect some change in our results. We will consider here the radial flow model, perhaps of the simplest of the complex flow cases possible [19], but it suffices to fully assess the impact of flow on our analysis.

We deal with the Doppler effect as follows: for a given pair of values T_f and v_c , the resulting m_\perp particle spectrum is obtained and analyzed using the spectral shape and procedure (error is proportional to spectral strength) employed by the experimental groups, and the theoretical inverse slope ‘temperature’ T_s^j is determined for each particle j which we can compare with the experimental results for T_s^j . Let us first address the case of S–W reactions. Here the strange (anti)baryon slopes are quite similar [8]. In consideration of, within error, overlapping values of T_s^j we decided to consider only one value $T_s = 235 \pm 10$, chosen near to the most precise fitted Lambda spectra slope. Once we find values of T_f and v_c , we can check how the slopes of all particles have fared. The resulting T_s^j are in remarkable agreement with experiment, well beyond what we expected: we find for kaons, lambdas and cascades the values $T_s^j = 215, 236$ and 246 MeV respectively, which both in trend and value agrees with the $K^0, \Lambda, \bar{\Lambda}, \Xi$ and $\bar{\Xi}$ WA85 results [8]: $T_s^{K^0} = 219 \pm 5$, $T_s^\Lambda = 233 \pm 3$, $T_s^{\bar{\Lambda}} = 232 \pm 7$, $T_s^\Xi = 244 \pm 12$ and $T_s^{\bar{\Xi}} = 238 \pm 16$.

Since the flow effect shifts particles of different mass differently into different domains of m_\perp, y , it is not surprising that the inclusion of flow only impacts the phase space abundance parameters, beyond their established errors. In the theory – experiment comparison the strategy case D remains the best, it has now (eliminating to simplify the analysis all redundant data points) $\chi^2/\text{dof} = 0.73$. Fit F has $\chi^2/\text{dof} = 0.83$, and thus we can conclude that the S–Au/W/Pb data is fully understood within

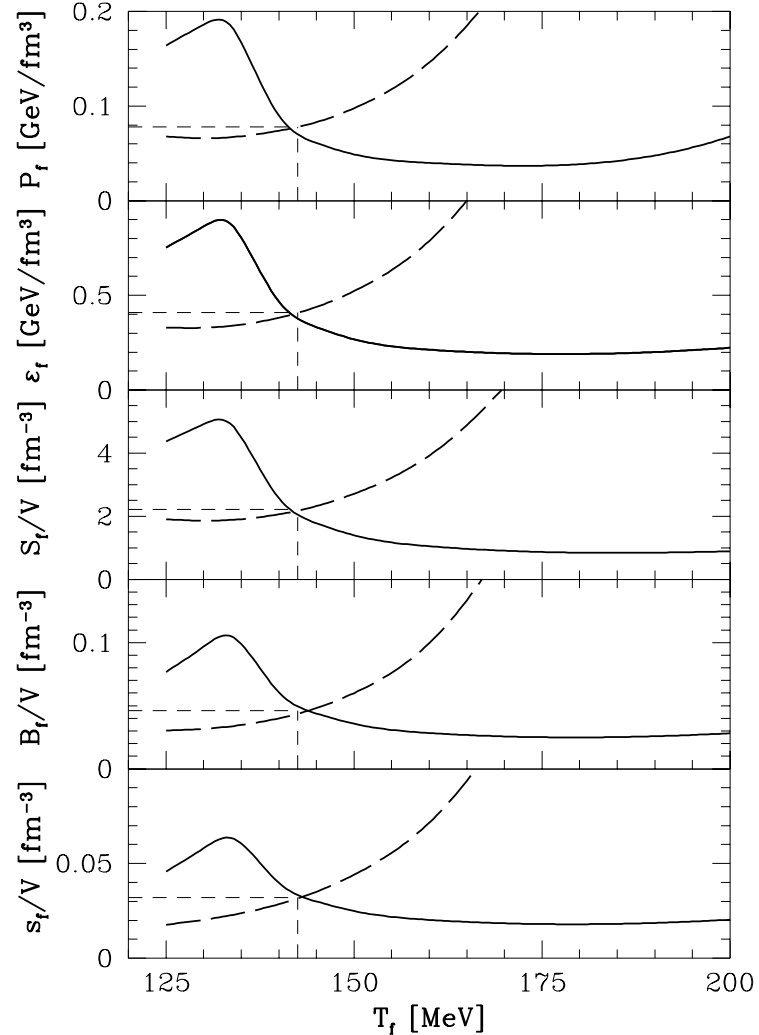


Figure 1. Comparison of the physical properties of the hadron source in Pb-Pb (solid lines) and S-Au/W/Pb (dashed lines) collision fireballs. Curves are obtained minimizing disagreement between theory and the experimental particle abundance data for a given T_f . We show in sequence from top to bottom: pressure P_f , energy density ϵ_f entropy density, S_f/V , baryon density B_f/V and s -quark density s_f/V .

the freeze-out non-equilibrium model with flow. In order to facilitate comparison with other work we note that to greater precision our case D with flow results for S-Au/W/Pb: $T = 142.7 \pm 2.1$ MeV, $\mu_b = 176 \pm 3$ and $|\vec{v}_c| = 0.486 \pm 0.010 c$. The situation allowing for strangeness non-conservation remains unchanged, case D_s with flow has negligible confidence level with $\chi^2/\text{dof} \simeq 3.2$. The strangeness imbalance in fits D, F is the same as we have obtained without flow, so this imbalance is not result of flow.

An interesting feature of case D with flow is that there is little correlation between now 6 theoretical parameters, in other words the flow velocity is a truly new degree

of freedom required by the experimental data and it helps attain a good agreement with experimental results. We also checked that nearly the same flow velocity is found when we only study the particle multiplicity, and disregard the information about the experimental inverse slope of m_{\perp} -spectra. It is for this reason that we present here the simple radial flow model, as within this scheme the inverse transverse slope of hadrons is correctly ‘predicted’ by the chemical freeze-out analysis with flow, and the systematic change of the individual Doppler-shifted slopes seems to be as described above, just right for different particles.

We note that in just one physical aspect consideration of collective flow offers a new insight: the value of γ_s we determine is compatible with unity. This value was noted already in the analysis of the S–S collision results [21], and so far eluded the analysis of S–W/Au/Pb collisions. Specifically, we find $\gamma_s/\gamma_q = 0.69 \pm 0.03$, $\gamma_q = 1.41 \pm 0.08$. Another result to note is that the specific energy per baryon when flow is present just needs the Lorentz factor γ_v to be nearly exactly the same as the result we found without flow, which was in fact just the available energy in the collision. This observation merely proves time and again the physical consistency of the statistical approach to particle abundance study.

We are presently completing a similar analysis of the Pb–Pb system which shall be reported in another paper [22]. Our findings are for this reaction case also fully compatible with the picture of the reaction we have been developing here, the major highlights of this work are that the collective radial flow velocity is fitted now to be just above, but compatible with the sound velocity of quark matter $v_c \simeq c/\sqrt{3} \simeq 0.6 c$. The chemical non-equilibrium parameters $\gamma_{q,s}$ are yet bigger, and exceed both value 2, the temperature at freeze-out increases slightly to 136–139 MeV from the value 133 MeV we saw in the case D without flow. The fugacities $\lambda_{q,s}$ remain unchanged. Despite further increase in the values of $\gamma_{q,s}$ we still find a smaller specific yield of $\bar{s}/b \simeq 0.7$ compared to the S–Au/W/Pb case. The higher collective velocity suggests as possible explanation the fact that the greater internal pressure reached in Pb–Pb collisions compared to S–Au/W/Pb case shortens the effective available time for strangeness production, resulting in lesser yield, despite a expected higher initial temperature [6]. A full report on these developments will also contain a possible resolution of Ω , $\overline{\Omega}$ high yield riddle exploiting a model involving gluon assisted production mechanism [22].

6. Current status and conclusions

We have presented detailed analysis of hadron abundances observed in central S–Au/W/Pb 200 A GeV and Pb–Pb 158 A GeV interactions within thermal equilibrium and chemical non-equilibrium phase space model of strange and non-strange hadronic particles. We assumed formation of a thermal dense matter fireball of a priori unknown structure, which explodes and disintegrates into the final state hadrons. This approach allows excellent description of all abundance data, and when flow is considered, also a good understanding of the transverse mass inverse slopes. For Pb–Pb system we have, depending on strategy we adopt, no less than 5 independent degrees of freedom, and a few more in S–Au/W/Pb reactions, and thus our approach is not a process of fitting an ‘elephant’ to a few data, but indeed it should be seen as a solid confirmation the chemical freeze-out as a well defined stage of the evolution of dense matter. We also find results that may indeed be of quite considerable importance for the search for quark-gluon plasma. In particular, the physical statistical parameters obtained here characterize a strange particle source which, both for S–Au/W/Pb and for Pb–Pb

case, when allowing for Coulomb deformation of the strange and anti-strange quarks, is exactly symmetric between s and \bar{s} quark carriers, as is natural for a deconfined state.

We find a highly significant description of all experimental data leading to a fireball having specific baryon energy $E/B \simeq 9$ GeV, high specific entropy $S/B \simeq 45-50$, and chemical freeze-out temperature $T_f \simeq 140$ MeV. The dense blob of matter was expanding in case of S-Au/W/Pb reactions with surface velocity $v_c \simeq 0.49c$ and in case of Pb-Pb reactions just nearly with sound velocity of quark matter $v_c \simeq c/\sqrt{3} \simeq 0.6c$. The near equilibrium abundance of strange quarks ($\gamma_s \simeq 1$, including flow), and the over-abundance of light quarks ($\gamma_q^2 \simeq 2$), is pointing to a deconfined, fragmenting quark-gluon fireball as the direct particle emission source.

Even though there is still considerable uncertainty about other freeze-out flow effects, such as longitudinal flow (memory of the collision axis), the level of consistency and quality of agreement between a wide range of experimental data and our chemical non-equilibrium, thermal equilibrium statistical model suggests that, for the observables considered here, these effects do not matter. Considering the quality of the data description obtained it is impossible to consider the results presented here as accidental and likely to see further major revision.

In conclusion, we have shown that strange particle production data, combined with the global hadron multiplicity (entropy), can be consistently interpreted within a picture of a hot hadronizing blob of matter governed by statistical parameters acquiring values expected if the source structure is that of deconfined QGP. We have further found that radial flow allows to account exactly for the difference between freeze-out temperature and the observed spectral shape, and allows full description of the inverse slope of m_\perp strange baryon and antibaryon spectra for S-induced reactions. The only natural interpretation of our findings is that these particles are emerging directly from hadronizing deconfined state and do not undergo a chemical re-equilibration after they have been produced.

Acknowledgments:

We thank E. Quercigh for interesting and stimulating discussions. This work was supported in part by a grant from the U.S. Department of Energy, DE-FG03-95ER40937. LPTHE, Univ. Paris 6 et 7 is: Unité mixte de Recherche du CNRS, UMR7589.

References

- [1] J. Letessier and J. Rafelski, submitted to *Phys. Rev. C*; [hep-ph/9806386], June 16, 1998.
- [2] J. Letessier, J. Rafelski and A. Tounsi, *Phys. Lett.* **B 410**, (1997) 315; [hep-ph/9710310]; J. Rafelski, J. Letessier, and A. Tounsi, *Acta Phys. Polon.*, **B28**, 2841, (1997); [hep-ph/9710340].
- [3] J. Letessier and J. Rafelski, [hep-ph/9807346], July 11, 1998.
- [4] R. Hagedorn, Suppl. Nuovo Cimento **2**, 147 (1965); Cargèse lectures in Physics, Vol. 6, Gordon and Breach (New York 1977) and references therein.
See also: J. Letessier, H. Gutbrod and J. Rafelski, *Hot Hadronic Matter*, NATO-ASI series B34,6 Plenum Press, New York 1995.
- [5] H. Grote, R. Hagedorn and J. Ranft, *Atlas of Particle Production Spectra*, (CERN-Service d'Information Scientifique, Geneva 1970).
- [6] J. Rafelski, J. Letessier and A. Tounsi, *Acta Phys. Pol. B* **27**, 1035 (1996), and references therein.

- [7] P. Braun-Munzinger, J. Stachel, J.P. Wessels and N. Xu, *Phys. Lett. B* **365**, 1 (1996); [nucl-th/9508020].
- [8] D. Evans for the WA85 Collaboration, APH N.S., Heavy Ion Physics **4**, 79 (1996) [proceedings of Strangeness 1996 – Budapest meeting].
- [9] E. Andersen *et al.*, WA97-collaboration, preprint CERN-EP-98-064, Apr 1998; *Phys. Lett. B* in press;
R. Calandro, WA97 collaboration, in this volume.
- [10] S.A. Bass *et al.*, *Prog. Part. Nucl. Phys.* **41**, 225 (1998); [nucl-th/9803035].
- [11] J. Rafelski, *Phys. Lett. B* **262**, 333 (1991); *Nucl. Phys. A* **544**, 279c (1992).
- [12] J. Letessier, A. Tounsi, U. Heinz, J. Sollfrank and J. Rafelski, *Phys. Rev. D* **51**, 3408 (1995), and references therein; [hep-ph/9212210].
- [13] J. Sollfrank, *J. Phys. G* **23**, 1903 (1997); [nucl-th/9707020], and references therein.
- [14] F. Becattini, M. Gazdzicki and J. Sollfrank, *Eur. Phys. J. C* **5**, 143 (1998); [hep-ph/9710529].
- [15] J. Rafelski, J. Letessier and A. Tounsi, Dallas–ICHEP (1992) p. 983 (QCD161:H51:1992); [hep-ph/9711350];
J. Letessier, A. Tounsi, U. Heinz, J. Sollfrank and J. Rafelski *Phys. Rev. Lett.* **70**, 3530 (1993); [hep-ph/9711349].
- [16] J. Letessier, A. Tounsi and J. Rafelski, *Phys. Rev. C* **50**, 406 (1994); [hep-ph/9711346];
J. Rafelski, J. Letessier and A. Tounsi, *Acta Phys. Pol. A* **85**, 699 (1994).
- [17] J. Rafelski and B. Müller, *Phys. Rev. Lett.* **48**, 1066 (1982); **56**, 2334E (1986).
- [18] T.S. Biro and J. Zimanyi *Phys. Lett. B* **113**, 6 (1982); *Nucl. Phys. A* **395**, 525 (1983).
- [19] E. Schnedermann, J. Sollfrank and U. Heinz, pp175–206 in *Particle Production in Highly Excited Matter*, NATO-ASI Series B303, H.H. Gutbrod and J. Rafelski, Eds., (Plenum, New York, 1993)
- [20] B. Muller and J. Rafelski, *Phys. Rev. Lett.* **34**, 349 (1975).
- [21] J. Sollfrank, M. Gaździcki, U. Heinz and J. Rafelski, *Z. Phys. C* **61**, 659 (1994).
- [22] J. Letessier and J. Rafelski, “Study of collective transverse flow and of gluon assisted $\Omega/\bar{\Omega}$ production in Pb–Pb collisions”, in preparation.